INTERNATIONAL JOURNAL OF AUTOMOTIVE AND MECHANICAL ENGINEERING
ISSN: 2229-8649 e-ISSN: 2180-1606
VOLUME 22, ISSUE 2, 2025, 12417 - 12429
DOI: https://doi.org/10.15282/ijame.22.2.2025.13.0950

RESEARCH ARTICLE

A Collision Risk Control Model for Mechanical Engineering Vehicles Based on Image Road Condition Monitoring Method

Hongyue Liu

School of Mechanical and Electrical, Shanghai Donghai Vocational and Technical College, 200241 Shanghai, China

ABSTRACT – Mechanical engineering vehicles play an important role in various construction projects, but they face various collision risks under different road conditions. To improve the safety of engineering vehicles in operation, a collision risk control model has been proposed. During the process, a generative adversarial network is used as the basis for designing image road condition monitoring methods. DeepLabv3+ is used for generator design, and ResNet101 is used as the encoder backbone network. Subsequently, the risk of vehicle collision is calculated using the artificial potential field method, and the repulsive field adjustment factor is introduced to adjust the repulsive force potential field function. The experiments confirmed that the research method remained below 294 k in parameter testing when the pixel size reached 50 M in two datasets. When testing the obstacle recognition accuracy, the research method achieved a recognition accuracy of 97.8% when obstacles accounted for 10% of the detection area during the day. When conducting obstacle avoidance success rate testing, the obstacle avoidance success rate of the research method remained above 94.7% when the proportion of obstacles in the detection area was 10%. These results confirmed that the research method had good operational performance and collision risk control effect, which could effectively reduce the collision risk of engineering vehicles. The main contribution of this study lies in the proposal of a collision risk control model for mechanical engineering vehicles based on image road condition monitoring and the optimization of the repulsive force potential field function, which solves the problem of local optima.

ARTICLE HISTORY
Received : 27th Aug. 2024
Revised : 08th Apr. 2025
Accepted : 15th May 2025
Published : 27th June 2025

KEYWORDS
Collision risk
Generative adversarial network
Artificial potential field
DeepLabv3+
Road condition monitoring

1. INTRODUCTION

Mechanical engineering vehicles often face collision risks when operating in complex road environments, leading to serious accidents that harm personal and property safety [1]. Therefore, it is necessary to study Collision Risk Control (CRC) to reduce the incidence of collision accidents and improve traffic safety levels. The acquisition of accurate road information and vehicle location data is crucial for rail transit. Currently, commonly used radar sensors may be affected by noise and malfunctions [2-3]. Traditional CRC makes it difficult to handle complex and ever-changing road conditions, requiring more efficient and adaptive methods [4-5]. CRC is related to the safety of people and mobile devices, and many experts have realized its importance. Some scholars have conducted relevant research on CRC. Yang et al. proposed a method based on compatibility constraints for the CRC of vehicles. This method controlled the safe distance between vehicles and obstacles by limiting uncertainty bias and introducing obstacle avoidance constraints, confirming its ability to perform more accurate risk identification [6]. De Marinis et al. proposed a method based on extension technology for obstacle avoidance in unmanned aerial vehicle piloting. They used two-dimensional path planning as the basis for a three-dimensional extension to achieve obstacle avoidance route calculation in three-dimensional space. These experiments confirmed that the proposed method had a good obstacle avoidance effect [7]. Chen et al. proposed a path planning-based CRC method for unmanned ground vehicles. They used quintic polynomial curves and robust output feedback control for path planning and tracking. The experiment confirmed that the method had a good obstacle-avoidance effect [8]. Shou et al. proposed an Artificial Potential Field (APF)-based method for obstacle avoidance in underwater robot formations. They used virtual structures to enhance the formation's organizational capabilities and neural networks to analyze the movement of organisms. The method was proven to have good formation obstacle avoidance accuracy [9]. Feng et al. proposed a tracking controller-based method for vehicle CRC. This method used APF to control safe distance, set threat levels to adjust repulsion, and used model predictive control to transform planned paths, demonstrating good risk control performance [10].

Some scholars have conducted relevant research on Road Condition Monitoring (RCM). Dewangan and Sahu proposed an RCM-based method for vehicle road analysis. They used neural networks as the technical basis for classifying road conditions and demonstrated the good sensitivity and accuracy of the method [11]. Du et al. proposed a deep-learning RCM for detecting road surface damage. They used various images captured by cameras as datasets and identified tasks through object detection algorithms, finding that the method has good applicability and computational speed [12]. Bhatia et al. proposed a method based on road condition image monitoring to address the issue of road pothole detection. They

*CORRESPONDING AUTHOR | H.Y. Liu | ✉ lhykk@126.com

used image data from different weather conditions and analyzed the images collected by thermal imaging technology, which showed good recognition accuracy [13]. Maeda et al. proposed a Generative Adversarial Network (GAN)-based image monitoring method for analyzing road damage situations. By manually collecting road damage images as training data, and then combining pine trees and ponies with GAN, it was verified that the method has good analytical performance [14]. Li et al. proposed an RCM based on transfer learning to address road surface damage detection. This method utilized GAN to transform the scene style of images and extracted image features through domain adaptation with good detection accuracy [15].

APF is a method that focuses on obstacle avoidance, with fast computational efficiency and the ability to meet the timeliness requirements of vehicles during CRC. Hao et al. proposed a two-dimensional collaborative vehicle formation model based on APF for the formation of autonomous driving fleets on urban roads. This model combined the elastic potential energy between vehicles and the transverse APF. The elastic potential energy between vehicles caused the vehicles in the convoy to attract each other at long distances and repel each other at close distances, thereby promoting lane changes. The lateral APF simulated lane-keeping behavior and provided resistance when lane-changing incentives were low. The simulation verified the effectiveness of the model and proved the rationality of behavior in typical driving scenarios, which can effectively handle vehicle obstacle avoidance and formation problems [16]. Chen et al. used APF for path planning and tracking control of fully controlled electric vehicles in unstructured scenarios, generating reference paths in scenes with different static obstacles and combining kinematic and dynamic constraints for speed planning. A path-tracking algorithm based on curvature calculation and model predictive control was designed, and a forward-looking behavior model with variable preview distance was constructed using fuzzy control theory. This method outperformed the tracking controller under high dynamic driving conditions, ensuring good dynamic tracking performance and maneuverability, and effectively solving the problem of vehicle obstacle avoidance [17].

Some calculation methods require high hardware requirements, and onboard systems generally do not have high hardware performance. GAN can achieve real-time image monitoring on the basis of commonly used imaging systems in vehicles, helping vehicles identify and analyze dangerous situations and obstacles in road conditions. Moreover, GAN is adaptable and can cope with different road and lighting conditions. In this context, based on the APF method, a mechanical engineering vehicle CRC model based on image RCM is designed using GAN, DeepLabv3+ network, and ResNet101 network. It aims to improve the effectiveness of safety control through pattern innovation and provide feasible technical references for vehicle safety control in engineering projects. The research content mainly has four sections. Firstly, the relevant research results of CRC and RCM are discussed. Secondly, a risk control model for engineering vehicle collisions based on image RCM is designed. The third section analyzes the effectiveness of the research method. Section 4 is a summary and discussion of the entire article. The contribution of the research lies in threefold. The first is to use GAN and DeepLabv3+ network combined with ResNet101 as the generation and encoder backbone to achieve efficient image semantic segmentation. Secondly, the dynamic environment of construction vehicles is abstracted as a potential field, and a potential field action range and hazard factor adjustment method represented in the form of a long axis ellipse is proposed to enhance the obstacle avoidance path planning and dynamic environment adaptability of construction vehicles. Thirdly, real-time road condition analysis and rail transit have been achieved in the engineering environment.

2. DESIGN OF ENGINEERING VEHICLE CRC BASED ON IMAGE RCM

2.1 Design of Road Condition Image Analysis Method Based on GAN

To improve the safety of engineering projects, the collision risk of engineering vehicles should be controlled. In most engineering environments, mechanical engineering vehicles have a large volume, and according to engineering safety requirements, vehicle speed is limited to a certain range. The common road conditions for engineering vehicles are shown in Figure 1.

Figure 1. Common road conditions for construction vehicles

Figure 1 shows that construction vehicles mainly have unpaved roads within the construction area and paved roads in the construction area and transportation sections. Most of the unpaved roads within the construction area are rugged and lack clear road boundary markers and driving guidance signs. When driving on such roads, drivers need to rely on their own experience to determine the appropriate driving strategy and path. However, large construction vehicles have a large blind spot in their field of vision, and there may be obstacles and dangerous factors entering the blind spot during driving, leading to collisions. In paved roads, the presence of other vehicles and pedestrians can also increase the risk of collision. The design of CRC model for large-volume mechanical engineering vehicles in an engineering environment with a vehicle speed limit is studied. Through image RCM, relevant road condition information can be provided for the vehicle control system, and GAN has a strong image semantic segmentation effect when analyzing road condition images [18-20]. GAN is used to design the image of the RCM in the vehicle CRC. The generator in GAN learns the true data distribution and establishes new samples that can directly reflect the data distribution [21-22]. Then, the discriminator distinguishes between new samples and real data, and alternates with the generator for optimization. The optimization is completed when the new samples generated by the generator are consistent with the real data. When conducting image RCM, the input road condition image is used to analyze the image content and obtain the corresponding road, obstacle, and other data in the image. The DeepLabv3+ generator in this study is shown in Figure 2.

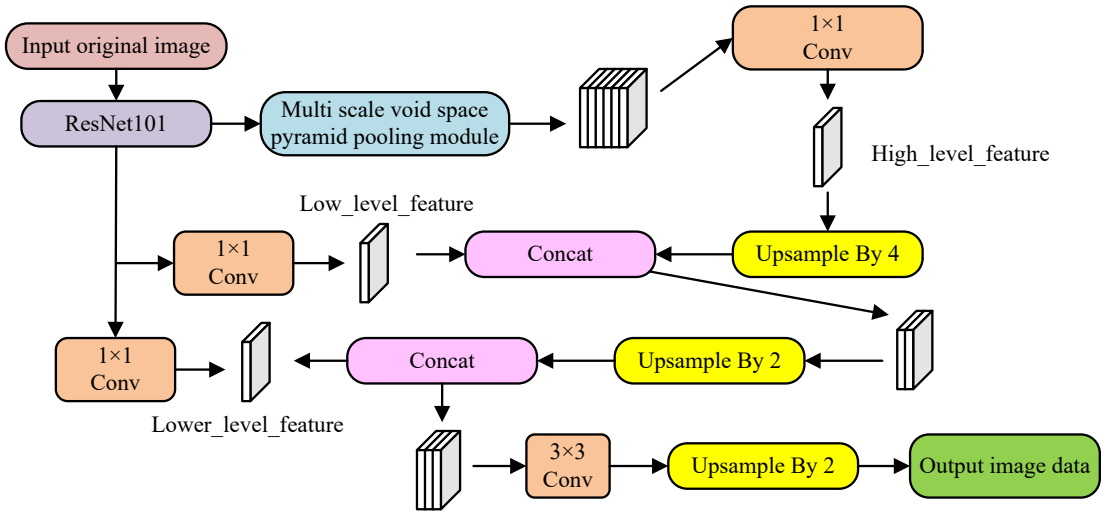

Figure 2. Generator DeepLabv3+

According to Figure 2, the generator DeepLabv3+ consists of encoder and decoder. In the encoder, ResNet101 serves as the backbone to enhance the inclusion of multi-scale branches in the feature extraction. Different sizes of average pooling operations are performed on the adjacent information of pixels in the input image to achieve image information extraction. The decoder is composed of a feature fusion network. After completing the learning of important features, it adjusts the channels and obtains feature maps with different channel numbers through feature fusion. Further up-sampling is performed to output image segmentation that matches the size of the input original image. In this case, the loss function of the generator is represented by Eq. (1).

$$\min\max f_t(D,G)=\mathrm{E}_{x\sim Pdata(x)}\left[\log\left(D(X)\right)\right]+\mathrm{E}_{z\sim pz(z)}\left[\log\left(1-D\left(G(z)\right)\right)\right] \tag{1}$$

In Eq. (1), D refers to the discriminator parameter. G refers to the generator parameter. E refers to the expected value. X refers to real environmental data. z refers to noise data in the image. $Pdata$ refers to the data distribution in the real environment. pz refers to the noise distribution. $D(X)$ refers to the output of the discriminator on real environmental data. $D\left(G(z)\right)$ refers to the output of the discriminator on the generated data. The discriminator network consists of four convolutional layers, which increase the depth of the image and reduce the image. After the image passes through all convolutional layers, the activation function $Sigmoid$ is used to calculate the probability that the input image is a real image. Eq. (2) is the Lipschitz condition in the discriminator.

$$\frac{\left|f(\chi)-f(\gamma)\right|}{\left|\chi-\gamma\right|}\le C \tag{2}$$

In Eq. (2), $f(\chi)$ and $f(\chi)$ represent the output of the discriminator. χ and γ represent the discriminator network inputs. C refers to a constant determined by the spectral norm. When the input and output of the discriminator conform to Lipschitz continuity, the training results of the discriminator tend to be more stable. Eq. (3) refers to the loss of the standard cross-entropy during GAN training.

$$L_c = -\sum_{h,w,c} b^l(h,w,c)\log G\left(a^l\right)(h,w,c) \tag{3}$$

In Eq. (3), L_c refers to the standard cross-entropy loss. h,w,c represent the size of the input image. b^l refers to the true label. a^l refers to labeled samples. $G(\cdot)$ refers to the generator's output data. Feature matching loss is used to minimize feature differences, as shown in Eq. (4).

$$L_{fm} = \left\| E_{\left(a^l,b^l\right)\sim D^l}\left[D_k\left(b^l \oplus a^l\right) - E_{a^u\sim D^u}\left[D\left(G\left(a^u\right)\oplus a^u\right)\right]\right]\right\| \tag{4}$$

In Eq. (4), L_{fm} refers to feature matching loss. D_k refers to the k-th layer of the discriminator. Eq. (5) refers to the self-training loss.

$$L_{st} = \begin{cases} -\sum_{h,w,c} b^* \log G\left(a^u\right), D\left(G\left(a^u\right)\right) \geq \gamma \\ 0, others \end{cases} \tag{5}$$

In Eq. (5), L_{st} refers to self-training loss. λ refers to the confidence threshold. b^* refers to a pseudo-label. Eq. (6) is the training loss function.

$$L_G = L_c + \delta_{fm}L_{fm} + \delta_{st}L_{st} \tag{6}$$

In Eq. (6), L_G refers to the training loss function. δ refers to the weighted coefficients of each function. In practical work, it is not advisable to be too frequently affected by unimportant ultra-small volume obstacles. In this study, obstacles with a maximum length exceeding 5 centimeters are identified as obstacles in all directions, otherwise, they are considered non-obstacles. When measuring distance based on images, the DeepLabv3+ network is used for semantic segmentation of images and classifying different regions in the image into roads, obstacles, and other elements. Next, by annotating the position of obstacles and the pixel features of the segmented area, combined with the camera's field of view and resolution information, the system estimates the actual distance from obstacles to vehicles through the spatial relationship between pixel points. The obtained GAN-based structure is represented in Figure 3.

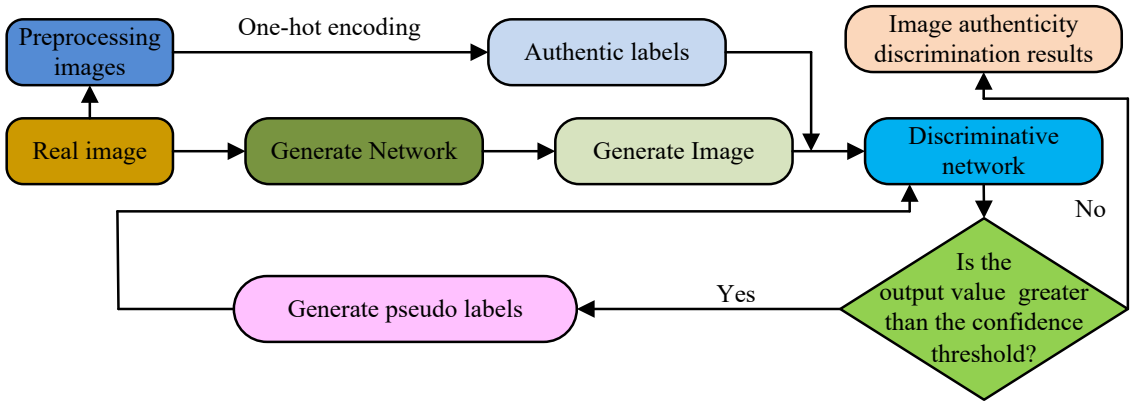

Figure 3. Generate adversarial network structure

According to Figure 3, when the network is running, the input road image is divided into two parts. One is input into the generated network, and the other is preprocessed and encoded to obtain the real label. After processing the image data in the input generation network by the generator, an image segmentation result that is consistent with the size of the original input image is obtained. The experiment inputs the real label, and the generator's processing results into the discriminator for discrimination. If the output exceeds the confidence threshold, a false label is generated and sent back to the discriminator for self-training. If the output does not exceed the confidence threshold, the true or false discrimination of the image annotation is output. After analyzing the road image data based on GAN, the collected road condition data is obtained.

2.2 Design of Automatic Control Technology for Vehicle Collision Risk Based on APF

When driving, in addition to avoiding fixed obstacles, it is also necessary to timely avoid moving targets that may appear on the road at any time. When evading, engineering vehicles have many constraints on their route selection due to the limitations of their working environment and body shape. APF has high real-time performance and easy parameter adjustment. The study chooses to use APF as the basis for designing automatic control technology for vehicle collision risk. By analyzing the output of road condition images, a repulsive potential field is assigned to the identified obstacles. Figure 4 shows the force model of the vehicle after being given a potential field.

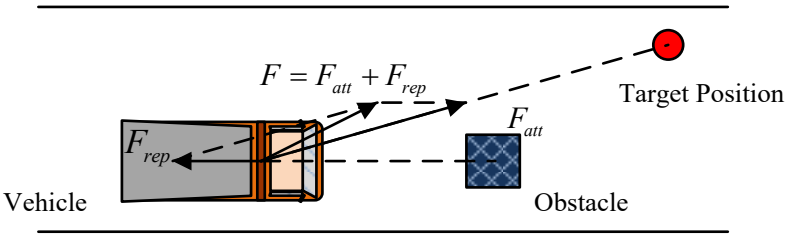

Figure 4. Vehicle force model given potential field

According to Figure 4, after the obstacle is given a repulsive field, the vehicle is subjected to a repulsive force from the obstacle during driving. The total force received is composed of the gravitational force at the target location and the repulsive force of the obstacle. Eq. (7) is the potential field function U .

$$U = U_{att} + U_{req} \tag{7}$$

In Eq. (7), U_{req} refers to the repulsive potential field function. U_{att} refers to the gravitational potential field function. When establishing the gravitational function, the driving environment is abstracted into a two-dimensional plane form, and the position coordinates of the vehicle and obstacle avoidance endpoint are set. The gravitational force on a vehicle is affected by the distance from the endpoint. Eq. (8) refers to the gravitational potential field.

$$U_{att} = \frac{1}{2} E_{att} \left(P_v - P_t \right)^2 \tag{8}$$

In Eq. (8), P_v refers to the vehicle position coordinates. P_t refers to the coordinates of the endpoint. E_{att} refers to the gain of the gravitational field. In the design of the gravity function, the driving environment is abstracted into a two-dimensional plane form. When optimizing the coordinates of the vehicle and obstacle avoidance endpoint, the gravity gain is adjusted according to the change in the distance from the target position to ensure that the vehicle can smoothly move toward the target. Eq. (9) is the gravitational function.

$$F_{att}(M) = -\nabla U_{att}(M) = -E_{att} \vec{a}_G l \tag{9}$$

In Eq. (9), F_{att} refers to gravity. $\vec{a}_G$ refers to the unit vector between the vehicle and the endpoint. l refers to the distance between the endpoint and the vehicle. When establishing the repulsion function, it is necessary to extract the position coordinates of obstacles. Eq. (10) refers to the repulsive potential field.

$$U_{req}(M) = \begin{cases} \frac{1}{2} E_{req} \left(\frac{1}{d_{ob}} - \frac{1}{d_0} \right)^2, d_{ob} \le d_0 \\ 0, d_{ob} > d_0 \end{cases} \tag{10}$$

In Eq. (10), d_{ob} refers to the distance between the obstacle and the vehicle. E_{req} refers to the gain of the repulsive field. d_0 refers to the domain of the repulsive field. By introducing adjustment factors and dynamically optimizing the repulsive field range, the repulsive field gain can be adjusted in real-time to adapt to different obstacle positions and risk levels, preventing the vehicle from getting stuck in local optima. Eq. (11) is the repulsive potential field function.

$$\begin{cases} F_{req}(M) = \begin{cases} \left(F_{req1} + F_{req2} \right)^2 \cdot \vec{a}_B, d_{ob} \le d_0 \\ 0, d_{ob} > d_0 \end{cases} \\ \begin{cases} F_{req1} = E_{req} \left(\frac{1}{d_{ob}} - \frac{1}{d_0} \right) \frac{1}{d_{ob}^2} \\ F_{req2} = \frac{n}{2} E_{req} \left(\frac{1}{d_{ob}} - \frac{1}{d_0} \right)^2 \end{cases} \end{cases} \tag{11}$$

In Eq. (11), $\vec{a}_B$ refers to the unit vector between the obstacle and the vehicle. In actual driving, the dynamic environment that vehicles face is complex. When subjected to the repulsive force of obstacles, the vehicle may experience a situation where the combined force is zero, resulting in the vehicle falling into a local optimum in Figure 5.

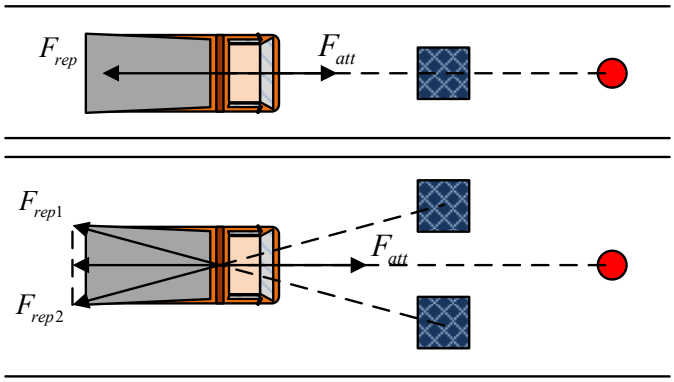

Figure 5. Local optimal dilemma

According to Figure 5, when an obstacle appears on the line connecting the vehicle and the endpoint path, reaching a certain position will result in a balance between gravity and repulsion. When obstacles appear on both sides of the line connecting the vehicle and the endpoint path, reaching a certain position will result in a combined lateral force of 0 between the two obstacles. The longitudinal component and combined force balance with the gravitational force on the vehicle. The increase in obstacles can make this situation more complex. To avoid the situation of resultant force balance, the study introduces a repulsive field adjustment factor to adjust the repulsive potential field function, which changes accordingly in Eq. (12).

$$U_{rep}(x,y)=\begin{cases}E_{rep}\left(\dfrac{1}{d(q,q_0)}-\dfrac{1}{d_0}\right)\rho, q\in\dfrac{(x-x_0)}{L_1}+\dfrac{(y-y_0)}{L_2}=1\\ 0, q\notin\dfrac{(x-x_0)}{L_1}+\dfrac{(y-y_0)}{L_2}=1\end{cases} \tag{12}$$

In Eq. (12), x_0, y_0 represent the position coordinate of the obstacle. L_1 refers to the distance on x axis. L_2 refers to the distance on y axis. ρ refers to the repulsion regulatory factor. The longitudinal movement ability of vehicles is significantly different from the lateral movement ability. Therefore, the repulsive potential field is designed in an elliptical form. The hazard coefficient is introduced to determine the long-axis length of the repulsive potential field's action range, as shown in Eq. (13).

$$L_c=\partial\cdot D_{\min} \tag{13}$$

In Eq. (13), L_c refers to the length of the long axis. ∂ refers to the risk factor. Figure 6 shows the force exerted by the road boundary on the vehicle.

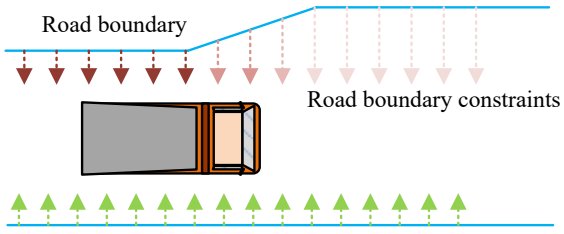

Figure 6. Road boundary forces

In Figure 6, the road boundary, as a strong constraint condition, has a sustained and strong force on the vehicle. When a vehicle approaches the road boundary, the force acting on the road boundary increases, prompting the vehicle to move away from the road boundary. Eq. (14) refers to the road boundary repulsion established in this context.

$$F_{road}(x,y)=\begin{cases}E_{road1}e^{-|y-y_l|}, y\le\dfrac{L}{4}\\ E_{road2}\cos\left(\dfrac{2(y-y_l)}{L}\right), \dfrac{L}{4}<y<\dfrac{3L}{4}\\ E_{road1}e^{|y-y_r|}, y\ge\dfrac{3L}{4}\end{cases} \tag{14}$$

In Eq. (14), F_{road} refers to the repulsive force of the road boundary on the vehicle. L_r refers to the width of the road. E_{road} refers to the potential energy coefficient of the road boundary. Eq. (15) refers to the combined force acting on the vehicle.

$$F(x,y)=F_{att}(x,y)+F_{rep}(x,y)+F_{road}(x,y) \tag{15}$$

In Eq. (15), $F(x,y)$ refers to the combined force acting on the vehicle. In the process of moving engineering vehicles, it is possible to enter a situation of dense vehicles and multiple obstacles, so the directed angle method is used to calculate the resultant force. In the process of movement, the next movement direction of the vehicle is jointly determined by the vehicle's running gear data and the steering wheel data, that is, the actual movement direction of the vehicle. The experiment will combine the designed CRC with existing vehicle imaging and automatic control systems, and run it in the onboard computer system to implement the research method. When training the model, the road environment image is first input into the generation network, which uses DeepLabv3+ as the generator and combines a ResNet101 encoder to extract multi-scale features, achieving efficient image semantic segmentation. Then, the generated image results are input into the discriminative network along with the real labels. The discriminative network distinguishes the generated image from the real image through multiple convolutional layers and continuously optimizes the generator and discriminator. During this process, the feature matching loss and cross-entropy loss function are utilized to enhance the segmentation accuracy of the generative network. Figure 7 shows the overall workflow of the research method.

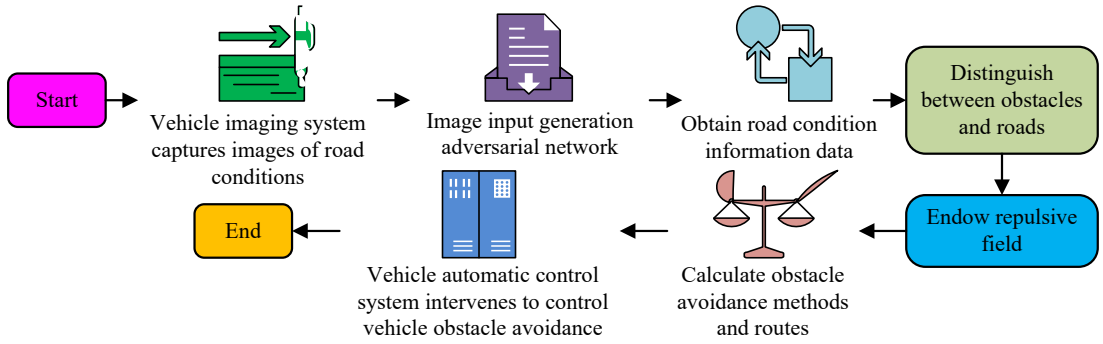

Figure 7. General process for vehicle collision risk control

According to Figure 7, when using the designed mechanical engineering vehicle CRC, the vehicle imaging system first collects and captures road condition images. Afterward, the captured image is input into the GAN to extract road conditions, and the image is segmented to distinguish obstacles and roads. After assigning APF to roads and obstacles, obstacle avoidance methods and routes are calculated. After inputting the calculation results into the vehicle's automatic control system, the vehicle's automatic control system intervenes to achieve obstacle avoidance.

3. EFFECTIVENESS ANALYSIS OF ENGINEERING VEHICLE CRC BASED ON IMAGE RCM

3.1 Performance Testing of Engineering Vehicle CRC Based on Image RCM

This section analyzed the software and hardware performance indicators of the designed engineering vehicle CRC during operation to confirm the theoretical feasibility of the research method. From the perspective of application analysis, the feasibility of the research method in practical environments was determined. The study analyzed the effectiveness of the image RCM-based CRC in engineering vehicles from two perspectives: performance and application. The road datasets Cityscapes and Camvid were used as test data for performance testing. Cityscapes included a total of 3,318 images, while Camvid included 601 images. During testing, comparisons were made with You Only Look Once Tiny (YOLO-Tiny) and CowMix. The Mean Intersection Over Union (MIoU) and runtime parameter values were tested in the experiment. Figure 8 shows the results in Cityscapes.

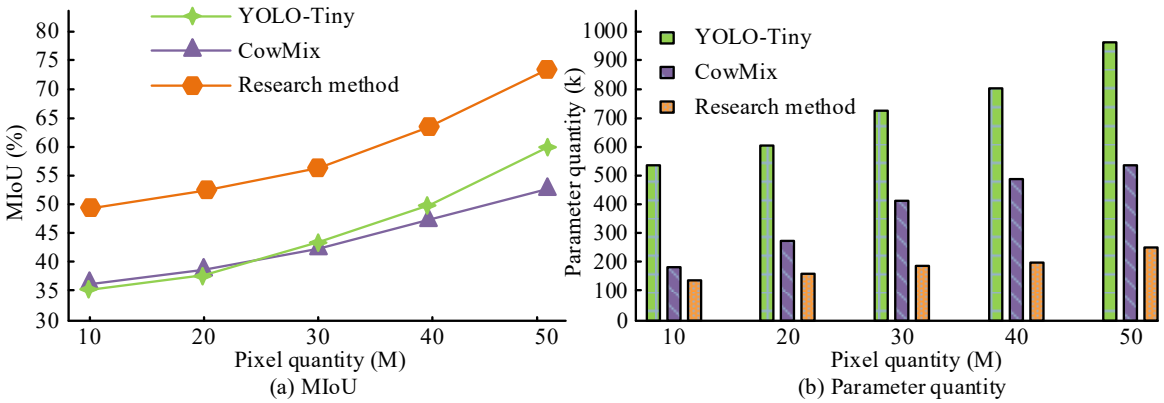

Figure 8. MIoU and parameter quantity in Cityscapes

According to Figure 8, the MIoU and parameter quantity of different methods increased with the increase of pixel size in Cityscapes. YOLO-Tiny's MIoU increased to 59.7% when the pixel increased to 50 M. The MIoU of CowMix increased to 52.6% when the pixel increased to 50 M. The MIoU of the research method increased to 49.4% when the pixel size was 10 M and to 73.1% when the pixel size increased to 50 M. The parameter quantity of YOLO-Tiny increased to 961 k when the pixel size increased to 50 M. The parameter counts of CowMix increased to 534 k when the pixel increased to 50 M. The parameter size of the research method was 127 k when the pixel size was 10 M and 249 k when the pixel size increased to 50 M. The standard deviation of MIOU data tested in the Cityscapes dataset was 0.4%. Figure 9 shows the results in Camvid.

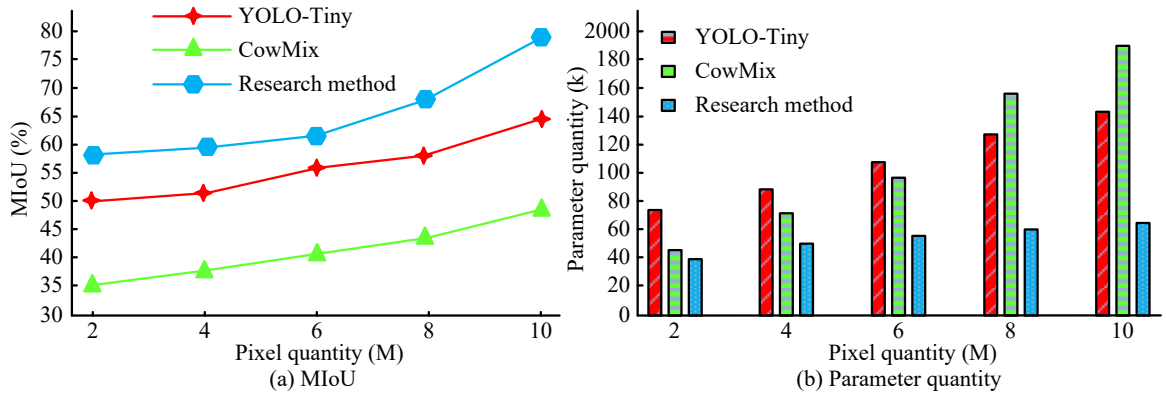

Figure 9. MIoU and parameter quantity in Camvid

According to Figure 9, the MIoU and parameter quantity of different methods increased with the increase of pixels in Camvid. YOLO-Tiny's MIoU increased to 64.7% when the pixel size reached 10 M. The MIoU of CowMix increased to 47.8% when the pixel size reached 10 M. The MIoU of the research method increased to 57.8% at 2 M pixels and 78.2% at 10 M pixels. YOLO-Tiny's parameter quantity increased to 143 k when the pixel size reached 10 M. The parameter quantity of CowMix increased to 189 k when the pixel size increased to 10 M. The parameter quantity of the research method increased to 39 k when the pixel size was 2 M and to 64 k when the pixel size increased to 10 M. This indicated that the research method had better model performance and could perform more accurate detection. Low parameter quantity brought less computational pressure to the running system and lower hardware requirements. The standard deviation of MIOU data tested in the Camvid dataset was 0.5%. Overall, image size had a significant impact on the variation of parameter quantity. As the number of image pixels increased, the model needed to process more detailed information, resulting in a synchronous increase in parameter count and computational complexity. On the Cityscapes dataset, as the pixel count increased from 10M to 50M, the parameter count of the research method increased from 127k to 249k. On the Camvid dataset, as the pixel count increased from 2 M to 10 M, the parameter count increased from 39 k to 64 k. In contrast, YOLO-Tiny and CowMix had higher parameter counts under the same pixel conditions, indicating that the research method significantly reduced parameter count and computational requirements by optimizing model design while maintaining high accuracy. This low parameter count made it more suitable for edge devices with limited hardware resources, ensuring real-time efficiency and enabling fast response even in high-resolution images. This advantage provided reliable support for the application of construction vehicles in complex dynamic environments. Floating Point Operations Per Second (FLOPS) values of the research method were tested in Figure 10.

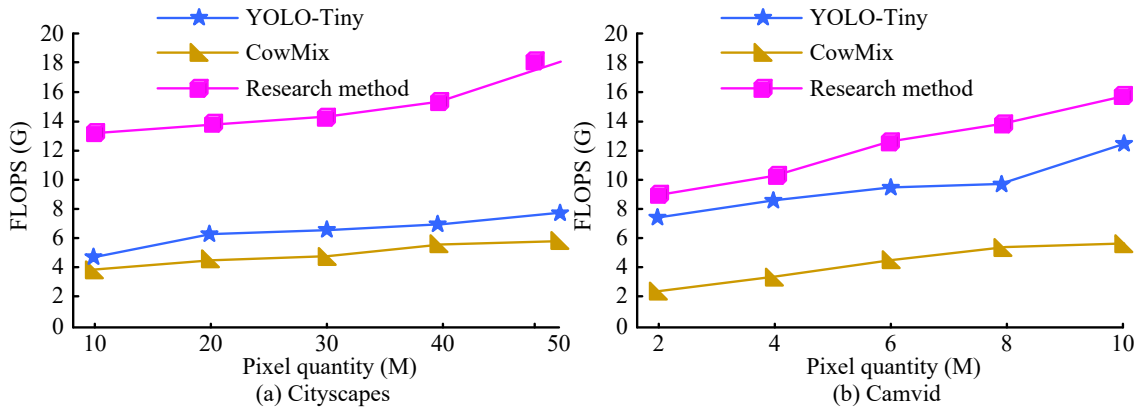

Figure 10. FLOPS test

According to Figure 10, the FLOPS of different methods all increased with the increase in pixels. In Cityscapes, YOLO-Tiny's FLOPS increased to 7.8 G when the pixel size reached 50 M. The FLOPS of CowMix increased to 5.9 G when the pixel size reached 50 M. The FLOPS of the research method was 13.2 G at 10M pixels and 18.0 G at 50 M

pixels. In Camvid, YOLO-Tiny's FLOPS rose to 12.3 G when the pixel reached 10 M. The FLOPS of CowMix increased to 5.6G when the pixel size reached 10 M. The FLOPS of the research method was 7.2 G at 2 M pixels and 15.7 G at 10 M pixels. The standard deviation of the FLOP value test data was 0.3G. This indicated that the research method had better computational speed and could respond more quickly when performing CRC.

3.2 Application Analysis of Engineering Vehicle CRC Based on Image RCM

When conducting application analysis, the Volvo FMX truck was used as the application test vehicle, and Autonomous Emergency Braking (AEB) was used as the execution system. Two application testing environments, daytime and nighttime, were set up. The accuracy of obstacle recognition in the system was tested in Figure 11.

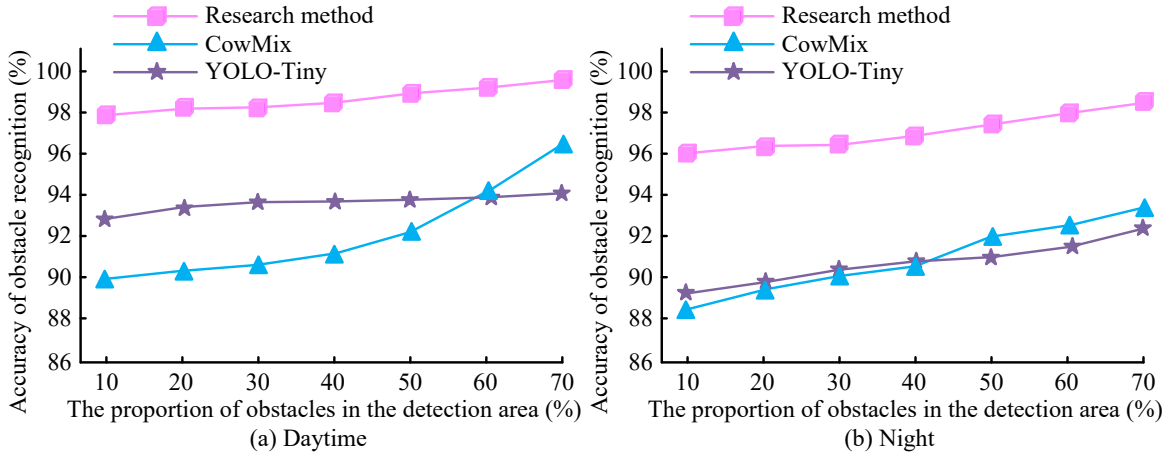

Figure 11. Accuracy of obstacle recognition

According to Figure 11, the accuracy of obstacle recognition by different methods in both daytime and nighttime increased with the proportion of obstacles in the detection area. During the day, YOLO-Tiny had a recognition accuracy of 94.2% when obstacles accounted for 70% of the detection area. The recognition accuracy of CowMix was 96.4% when the proportion of obstacles in the detection area was 70%. The recognition accuracy of the research method was 97.8% when the proportion of obstacles was 10%, and increased to 99.6% when the proportion increased to 70%. At night, YOLO-Tiny had a recognition accuracy of 92.5% when obstacles accounted for 70% of the detection area. The recognition accuracy of CowMix was 93.4% when the proportion of obstacles was 70%. The recognition accuracy of the research method was 95.9% when the proportion of obstacles was 10%, and when the proportion increased to 70%, the accuracy increased to 98.4%. This indicated that the research method could maintain high accuracy in obstacle recognition in both daytime and nighttime, providing better data assurance for subsequent obstacle avoidance. Moreover, in all kinds of engineering construction scenes, not only the two types of daylight and night lighting states, but also some engineering vehicles need to frequently enter and exit the tunnel and frequently switch between different lighting environments. The research method had good recognition accuracy in both day and night representative light environments and could also accurately identify obstacles in other light environments to ensure that engineering vehicles can accurately avoid obstacles during the working process. The calculation time of the system's risk control method was tested in Figure 12.

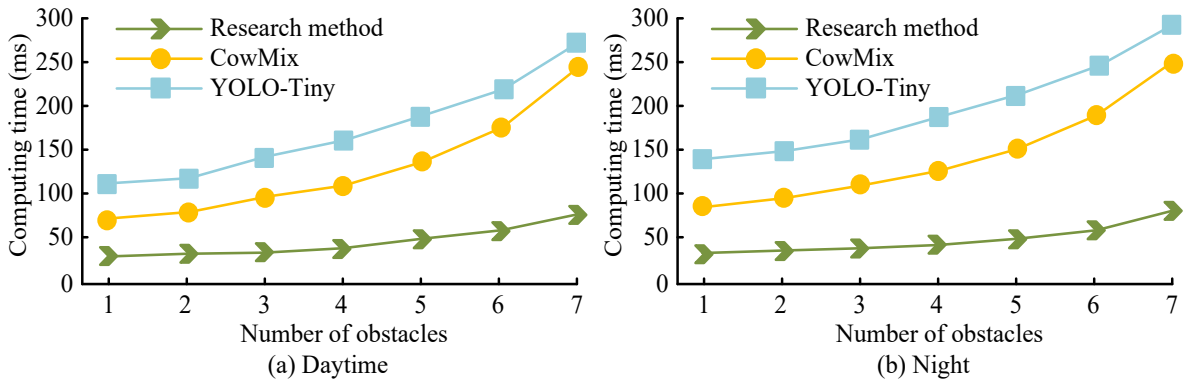

Figure 12. Method calculation time

According to Figure 12, the calculation time of different methods increased with the increase in obstacles. During the day, YOLO-Tiny's calculation time when there were 7 obstacles was 273 ms. The calculation time for CowMix when there were 7 obstacles was 247 ms. The calculation time for the research method was 28 ms when there was one obstacle, and 75 ms when the number increased to 7. At night, YOLO-Tiny's calculation time when there were 7 obstacles was 291 ms. The calculation time for CowMix when there were 7 obstacles was 249 ms. The calculation time for the research

method was 30 ms when there was one obstacle, and it increased to 78 ms when the number of obstacles increased to 7. The research method had a faster calculation speed for risk control, providing more execution space for obstacle avoidance operations. More engineering vehicles had greater mass and greater inertia, and earlier operations could reduce the occurrence of sudden turns and sudden stops when avoiding obstacles. There would also be fewer instances of uncontrollable hazards during obstacle avoidance. Figure 13 analyzes the success rate of obstacle avoidance.

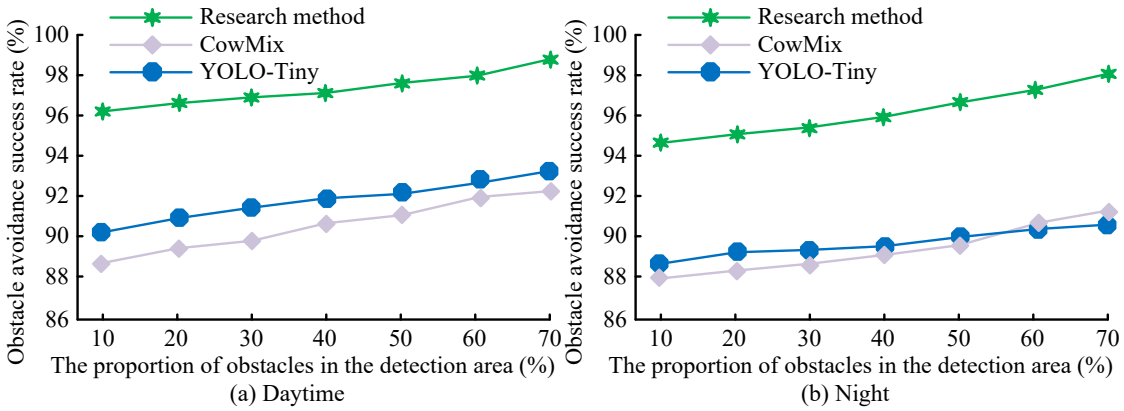

Figure 13. Obstacle avoidance success rate

In Figure 13, the success rate of obstacle avoidance for different methods increased with the proportion of obstacles in the detection area. During the day, YOLO-Tiny achieved a success rate of 93.1% when obstacles accounted for 70% of the detection area. CowMix's obstacle avoidance success rate was 92.2% when the proportion of obstacles was 70%. The success rate of obstacle avoidance was 96.2% when the proportion of obstacles was 10%. When the proportion increased to 70%, the success rate increased to 98.8%. At night, YOLO-Tiny achieved a success rate of 90.4% when obstacles accounted for 70%. CowMix's obstacle avoidance success rate was 91.3% when the proportion of obstacles was 70%. The success rate of obstacle avoidance was 94.7% when the proportion of obstacles was 10%. When the proportion increased to 70%, the success rate increased to 98.1%. The research method had a higher success rate in obstacle avoidance and a better CRC effect. In the engineering environment, a higher success rate of obstacle avoidance could bring a higher engineering safety factor and reduce the safety accidents caused by improper control of engineering vehicles. The study conducted an uncertainty analysis on model parameters using the Monte Carlo simulation method. In the simulation, 1,000 random samples were taken, and different parameter sets were used for each simulation. These parameter sets were randomly selected from the posterior distribution of the model parameters. Research has found that the uncertainty of model predictions mainly comes from the accuracy of obstacle recognition, especially under low-lighting conditions.

In this case, the standard deviation of the model's prediction error was approximately 3.2%. To quantify the reliability of model predictions, confidence intervals were calculated. In the test where the proportion of obstacles in the detection area during the day was 10%, the 95% confidence interval of the obstacle recognition accuracy of the research method was 97.8%±1.2%. This meant that there was a 95% confidence that the accuracy of the research method was at least 96.6% (97.8%-1.2%) and would not be lower than 95.4% (97.8%-2.4%). In nighttime testing, the uncertainty of research methods increased due to changes in environmental lighting conditions. When the proportion of obstacles in the detection area was 10%, the 95% confidence interval of the obstacle recognition accuracy of the research method was 95.9%± 1.5%. This indicated that the accuracy of the research method in nighttime environments was at least 94.4%. The study calculated the Mean Square Error (MSE) and Root Mean Square Error (RMSE) between the predicted values of the model and the actual collision risk. In all testing scenarios, the average value of MSE was 0.02, and the average value of RMSE was 0.15, indicating a small deviation between the model's predictions and actual observations. Sensitivity testing was conducted on the key parameters of the model, including the threshold for obstacle detection and the adjustment factor for the field. By changing these parameters, the study found that the predicted collision risk of the model fluctuated within the range of ± 3%, indicating that the model has a certain degree of robustness to changes in these parameters. However, when the obstacle detection threshold was set too low, the false alarm rate of the model significantly increased, indicating that these parameters needed to be carefully adjusted in practical applications to balance accuracy and robustness. To further determine the superiority of the research method, a comparison was made between the recently proposed Optimal reinforcement learning [23] and Cooperative Obstacle Avoidance [24] in the same scenario, as shown in Table 1.

As shown in Table 1, the obstacle recognition accuracy of the research method is higher than that of other comparative methods in both daytime and nighttime tests. The research method requires significantly fewer parameters (39k-64k), which greatly reduces computational overhead compared to Optimal reinforcement learning (189k) and Cooperative Obstacle Avoidance (143k), making it more suitable for edge devices with limited resources. The research method shows the fastest calculation speed (28ms to 75ms) when dealing with 1 to 7 obstacles, ensuring real-time decision-making ability, especially suitable for heavy engineering vehicles with high inertia. In low-light environments, the proposed method maintains 95.4% robustness, while Optimal reinforcement learning and Cooperative Obstacle Avoidance decrease

to 88.3% and 91.1%, respectively. Its RMSE is only 0.15, indicating minimal deviation in the predicted results. The stronger practical application performance of the research method is demonstrated.

Table 1. Comparison of actual advanced technologies

Metrics	Research Method	Optimal reinforcement learning	Cooperative Obstacle Avoidance
Accuracy of Obstacle Recognition	Day: 97.8% (10% obstacles), Night: 95.9% (10% obstacles)	Day: 93.6% Night: 89.4%	Day: 94.2% Night: 91.5%
Obstacle Avoidance Success Rate	Day: 96.2% (10%) – 98.8% (70%) Night: 94.7% (10%) – 98.1% (70%)	Day: 90.8% – 96.5% Night: 87.5% – 94.8%	Day: 91.7% – 97.1% Night: 89.2% – 95.5%
Model Parameter Count	39k–64k	189k	143k
Processing Speed (ms)	28ms (1 obstacle) – 75ms (7)	63ms (1) – 247ms (7)	58ms (1) – 273ms (7)
Computation (FLOPS)	7.2G – 18.0G	9.5G – 21.3G	8.2G – 19.6G
Detection Robustness (Low Light)	95.40%	88.30%	91.10%
Collision Avoidance Efficiency	High – Optimized via APF adjustments	Moderate – Policy-based optimization	Moderate
System Resource Efficiency	Low (optimized for edge devices)	Moderate (requires hardware tuning)	Moderate
Adaptability to Complex Obstacles	High	Moderate	Moderate
Error Rate (RMSE)	0.15	0.23	0.19

4. DISCUSSION AND CONCLUSION

Controlling the collision risk of mechanical engineering vehicles can improve the safety of engineering projects. The study proposed a mechanical engineering vehicle CRC based on image RCM to improve the safety of mechanical engineering vehicles. During the process, the road condition image was input to obtain the corresponding road, obstacle and other data in the image. The generator used the DeepLabv3+ network, composed of an encoder and decoder, to design the loss function for generating the antagonism network and used the activation function to calculate the true probability of the image. Then, the image was marked through the network to get the traffic data. The obstacle was given a repulsive potential field, and the repulsive potential field function was adjusted to avoid the resultant equilibrium. The automatic control technology was implemented through the vehicle system, and the effectiveness of the method was analyzed. The experimental results showed that the MIoU value of the research method remained above 49.4% in two datasets with a pixel size of 10 M, mainly due to the DeepLabv3+ using ResNet101 as the backbone network of the encoder, which enhanced the model's ability to capture multi-scale features. When conducting FLOPS testing, the research method could reach a maximum of 15.7 G when the pixel size reached 10 M. The research method achieved a recognition accuracy of 98.4% when obstacles accounted for 70% of the detection area in nighttime environments. In the daytime environment, the calculation time of the research method was only 75 ms when the number of obstacles increased to 7. The success rate of obstacle avoidance in the research method reached a maximum of 98.8% when the proportion of obstacles in the detection area was 70%.

This was mainly because the adjustment mechanism studied enabled vehicles to adjust their obstacle avoidance strategies in real-time based on the position and risk level of obstacles, effectively avoiding local optima problems. The above results showed that the research method could reduce the collision accidents caused by operation errors of construction vehicles by real-time monitoring of road conditions and calculation of collision risk. The accuracy of the collision risk assessment capability of research methods could help vehicles plan safer driving paths and avoid unnecessary parking and delays, thereby improving the overall efficiency of construction operations. The research method could reduce the occurrence of collision accidents, thereby directly reducing the maintenance and replacement costs caused by vehicle damage and saving valuable resources for engineering projects. It showed that the research method had broad prospects in practical engineering applications. However, the research method had only been tested on wheeled engineering vehicles, and the application effect in tracked vehicles was not yet clear. In the future, the application effect of the research method in tracked vehicles will be analyzed, and the method will be optimized. Future research will consider the performance of obstacles under non-static conditions and the impact of road conditions on vehicle dynamic performance. The research will expand to analyze the obstacle avoidance strategies of vehicles when facing moving obstacles and explore in depth the impact of different road conditions on vehicle handling performance and stability. In addition, the accuracy of the model and the effectiveness of obstacle avoidance strategies will be verified through real

vehicle experiments, while exploring multi-sensor data fusion technology. In the future, the accuracy and robustness of obstacle recognition will be improved, and vehicle control systems will be optimized to adapt to various complex environments, thereby enhancing the safety and efficiency of construction vehicles.

ACKNOWLEDGEMENTS

The author would like to acknowledge the Shanghai Donghai Vocational and Technical College for the research support.

CONFLICT OF INTEREST

The author declares no conflicts of interest.

REFERENCES

[1] D. Arya, H. Maeda, S. K. Ghosh, D. Toshniwal, and Y. Sekimoto, "RDD2022: A multi-national image dataset for automatic road damage detection," *Geoscience Data Journal*, vol. 11, no. 4, pp. 846-862, 2024.

[2] S. Ghanem, P. Kanungo, G. Panda, S. C. Satapathy, and R. Sharma, "Lane detection under artificial colored light in tunnels and on highways: An IoT-based framework for smart city infrastructure," *Complex and Intelligent System*, vol. 9, no. 4, pp. 3601-3612s, 2023.

[3] S. Jana, A. I. Middya, and S. Roy, "Participatory sensing based urban road condition classification using transfer learning," *Mobile Networks and Applications*, vol. 29, no. 1, pp. 42-58, 2024.

[4] C. A. Thieme, B. Rokseth, and I. B. Utne, "Risk-informed control systems for improved operational performance and decision-making," *Proceedings of the Institution of Mechanical Engineers, Part O: Journal of Risk and Reliability*, vol. 237, no. 2, pp. 332-354, 2023.

[5] A. Rawson and M. Brito, "A survey of the opportunities and challenges of supervised machine learning in maritime risk analysis," *Transport Reviews*, vol. 43, no. 1, pp. 108-130, 2023.

[6] H. Yang, Q. Li, Z. Zuo, and H. Zhao, "Event-triggered model predictive control for multi-vehicle systems with collision avoidance and obstacle avoidance," *International Journal of Robust and Nonlinear Control*, vol. 31, no. 11, pp. 5476-5494, 2021.

[7] A. De Marinis, F. Iavernaro, and F. Mazzia, "A minimum-time obstacle-avoidance path planning algorithm for unmanned aerial vehicles," *Numerical Algorithms*, vol. 89, no. 4, pp. 1639-1661, 2022.

[8] Y. Chen, C. Hu, Y. Qin, M. Li, and X. Song, "Path planning and robust fuzzy output-feedback control for unmanned ground vehicles with obstacle avoidance," *Proceedings of the Institution of Mechanical Engineers, Part D: Journal of Automobile Engineering*, vol. 235, no. 4, pp. 933-944, 2021.

[9] Y. Shou, B. Xu, H. Lu, A. Zhang, and T. Mei, "Finite-time formation control and obstacle avoidance of multi-agent system with application," *International Journal of Robust and Nonlinear Control*, vol. 32, no. 5, pp. 2883-2901, 2022.

[10] S. Feng, Y. Qian, and Y. Wang, "Collision avoidance method of autonomous vehicle based on improved artificial potential field algorithm," *Proceedings of the Institution of Mechanical Engineers, Part D: Journal of Automobile Engineerin*g, vol. 235, no. 14, pp. 3416-3430, 2021.

[11] D. K. Dewangan and S. P. Sahu, "RCNet: Road classification convolutional neural networks for intelligent vehicle system," *Intelligent Service Robotics*, vol. 14, no. 2, pp. 199-214, 2021.

[12] Y. Du, N. Pan, Z. Xu, F. Deng, Y. Shen, and H. Kang, "Pavement distress detection and classification based on YOLO network," *International Journal of Pavement Engineering*, vol. 22, no. 13, pp. 1659-1672, 2021.

[13] Y. Bhatia, R. Rai, V. Gupta, N. Aggarwal, and A. Akula, "Convolutional neural networks based potholes detection using thermal imaging," *Journal of King Saud University-Computer and Information Sciences*, vol. 34, no. 3, pp. 578-588, 2022.

[14] H. Maeda, T. Kashiyama, Y. Sekimoto, T. Seto, and H. Omata, "Generative adversarial network for road damage detection," *Computer-Aided Civil and Infrastructure Engineering*, vol. 36, no. 1, pp. 47-60, 2021.

[15] Y. Li, P. Che, C. Liu, D. Wu, and Y. Du, "Cross-scene pavement distress detection by a novel transfer learning framework," *Computer-Aided Civil and Infrastructure Engineering*, vol. 36, no. 11, pp. 1398-1415, 2021.

[16] R. Hao, M. Liu, W. Ma, B. Van Arem, and M. Wang, "A flock-like two-dimensional cooperative vehicle formation model based on potential functions," *Transportmetrica B: Transport Dynamics*, vol. 11, no. 1, pp. 174-195, 2023.

[17] G. Chen, M. Hua, W. Liu, J. Wang, S. Song, C. Liu, et al., "Planning and tracking control of full drive-by-wire electric vehicles in unstructured scenario," *Proceedings of the Institution of Mechanical Engineers, Part D: Journal of Automobile Engineering*, vol. 238, no. 13, pp. 3941-3956, 2024.

[18] D. K. Dewangan and S. P. Sahu, "PotNet: Pothole detection for autonomous vehicle system using convolutional neural network," *Electronics Letters*, vol. 57, no. 2, pp. 53-56, 2021.

[19] P. Singh, A. E. Kamal, A. Bansal, and S. Kumar, "Road pothole detection from smartphone sensor data using improved LSTM," *Multimedia Tools and Applications*, vol. 83, no. 9, pp. 26009-26030, 2024.

[20] T. Yamaguchi and T. Mizutani, "Quantitative road crack evaluation by a U-Net architecture using smartphone images and Lidar data," *Computer-Aided Civil and Infrastructure Engineering*, vol. 39, no. 7, pp. 963-982, 2024.

[21] S. Kumar and A. Sikander, "A modified probabilistic roadmap algorithm for efficient mobile robot path planning," *Engineering Optimization*, vol. 55, no. 9, pp. 1616-1634, 2023.

[22] X. Kong, H. Yuan, X. Zou, Y. Zhao, and S. Xiu, "A dynamic temperature condition monitoring method by vibration signal in grinding process," *The International Journal of Advanced Manufacturing Technology*, vol. 131, no. 5, pp. 2497-2507, 2024.

[23] H. Taghavifar, L. Taghavifar, C. Hu, C. Wei, and Y. Qin, "Optimal reinforcement learning and probabilistic-risk-based path planning and following of autonomous vehicles with obstacle avoidance," *Proceedings of the Institution of Mechanical Engineers, Part D: Journal of Automobile Engineering*, vol. 238, no. 6, pp. 1427-1439, 2024.

[24] D. Zhai, D. Yang, J. Chen, Z. Luo, M. Yu, and Z. Zhou, "Model for the cooperative obstacle‐avoidance of the automated vehicle swarm in a connected vehicles environment," *IET Intelligent Transport Systems*, vol. 17, no. 6, pp. 1137-1151, 2023.